Volume 121
Number 6
March 15, 2022

Biophysical Journal

Bringing physics to life

www.biophysj.org

Biophysical Society

CellPress
Partner Journal

Biophysical Journal
Article

Biophysical Society

Cell twisting during desiccation reveals axial asymmetry in wall organization

Sedighe Keynia,[1] Thomas C. Davis,[2] Daniel B. Szymanski,[2] and Joseph A. Turner[1,*]
[1]Mechanical and Materials Engineering, University of Nebraska-Lincoln, Lincoln, Nebraska and [2]Department of Botany and Plant Pathology, Department of Biological Sciences, Purdue University, West Lafayette, Indiana

ABSTRACT Plant cell size and shape are tuned to their function and specified primarily by cellulose microfibril (CMF) patterning of the cell wall. *Arabidopsis thaliana* leaf trichomes are unicellular structures that act as a physical defense to deter insect feeding. This highly polarized cell type employs a strongly anisotropic cellulose wall to extend and taper, generating sharply pointed branches. During elongation, the mechanisms by which shifts in fiber orientation generate cells with predictable sizes and shapes are unknown. Specifically, the axisymmetric growth of trichome branches is often thought to result from axisymmetric CMF patterning. Here, we analyzed the direction and degree of twist of branches after desiccation to reveal the presence of an asymmetric cell wall organization with a left-hand bias. CMF organization, quantified using computational modeling, suggests a limited reorientation of microfibrils during growth and a maximum branch length limited by the wall axial stiffness. The model provides a mechanism for CMF asymmetry, which occurs after the branch bending stiffness becomes low enough that ambient bending affects the principal stresses. After this stage, the CMF synthesis results in a constant bending stiffness for longer branches. The bending vibration natural frequencies of branches with respect to their length are also discussed.

SIGNIFICANCE The growth of plant cell walls is governed by the direction of cellulose synthesis, but the factors that influence the overall wall anisotropy are only partially understood. The twist of leaf trichome branches after desiccation reveals a left-handed asymmetry in cell wall organization even though the geometry is axisymmetric. This surprising behavior provides information about the directionality of cellulose synthesis control in plant cells.

INTRODUCTION

The shape and growth pattern of a plant cell are determined by the organization of cellulose microfibrils (CMFs) (1–4), the major load-bearing components within cell walls that are needed to constrain the relatively high (~5–10 atm) hydrostatic turgor pressure. The remaining cell wall volume consists of a hydrated matrix of pectin, hemicelluloses, and structural proteins (5,6). According to the cellulose synthase constraint hypothesis (7,8), cortical microtubules and associated proteins control the synthesis of CMFs, and microtubule orientation has been correlated with plant cell wall stresses during morphogenesis (9–13). Thus, tracking of microtubules is often used to reveal information about CMF organization during growth and the anisotropic mechanical properties that arise from their orientation.

According to the multinet growth hypothesis (14,15), CMFs realign to the direction of maximum stress. Unfortunately, it is not possible to measure stress in cell walls directly, so computational models are needed to match measured load-displacement and/or strain data to infer mechanical behavior. Then, model stress patterns can be used to reveal relations between microtubules and CMFs. Such analyses for most plant tissues are complicated by cell-cell interactions because boundary conditions are challenging to estimate. For this reason, isolated, unicellular structures, such as the leaf trichomes studied here, provide valuable insight into the role of stress and cytoskeleton-patterned cell wall heterogeneity for polarized cell growth (16).

The organization of cell wall constituents controls the wall mechanical behavior. In particular, the orientation distribution of CMFs is critical to the determination of wall strain and the growth patterns under turgor pressure (6). However, when the turgor pressure is removed, the resulting deformation can reveal organization information that cannot be determined from the pressurized cell alone. A similar

Submitted August 27, 2021, and accepted for publication February 9, 2022.
*Correspondence: jaturner@unl.edu
Editor: Guy Genin.
https://doi.org/10.1016/j.bpj.2022.02.013

concept is used in biomedical engineering to study the material behavior of arteries (17,18). An artery is a pressurized composite tube composed of smooth muscle cells, elastin, and collagen, each with different mechanical properties. Growth and remodeling in the loaded state of the artery produce stresses for the unloaded state. When a single axial cut is made in an unloaded artery, the cross-section opens at a specific angle because of residual stress in the artery wall. We exploit a similar concept through the removal of turgor pressure by desiccation; once the pressure is removed, the cell deformation reflects the stress state under pressure. Hence, by using a computational approach (cell wall deformation after dehydration and stress release) along with the experimental measurements, concepts about organization, such as the multinet growth hypothesis, can be investigated.

In addition, recent studies of trichome dynamics (19,20) used finite element (FE) models to predict the natural frequencies associated with the modes of bending vibrations. Their results were interpreted with respect to trichome functionality against herbivore insects and were analyzed relative to the sounds generated by the insects, but their predicted frequencies were higher than the range from many insects. However, their FE models were based on an isotropic material with mechanical properties that were constant during growth. Clearly, more accurate material information would improve the predicted vibration behavior.

In this article, desiccation of leaf trichome branches is used to quantify the cell wall mechanical properties using a computational model that reproduces the experimental deformations. The model is then used to understand changes in the axial stiffness, bending stiffness, and vibrational natural frequencies of the branch during growth. The stiffnesses define the capacity of the branch to deformation for a specific loading direction, and the natural frequency has been suggested as a defensive mechanism against environmental threats from insects. The results are expected to impact future studies focused on the role of genetics and/or environment on plant growth and development. Specifically, other important trichoblasts include cotton fibers (21,22), for which small advances in modeling efforts could have a dramatic impact on the global textile industry through identification of genetic modifications that can enhance fiber performance metrics. Computational approaches, when effectively integrated with advanced biological methods, may allow new crop varieties to be developed efficiently.

MATERIALS AND METHODS

Microtubule imaging and microtubule orientation quantification

Plate-grown Col-0 seedlings carrying a transgenic UBQ1p:TUB6-RFP construct were used for imaging trichomes on leaves 3 to 5. Briefly, images were acquired on a spinning disk confocal microscope with a 100×1.4 NA oil immersion objective, using a 561-nm solid-state laser as previously described (16). Several partially overlapping image stacks were acquired along the long axis of the cell to capture the whole trichome branch. Individual image stacks for a given branch were stitched together using the image montaging and alignment approach (Slidebook Software, Intelligent Imaging Innovations, Denver, CO). This approach allowed us to image one-half of the branch volume along its entire length. The expression level of the TUB6-RFP was low, and laser power was also optimized to enable repeated imaging without bleaching. The resulting images were adjusted for brightness and contrast. The 15-pixel-radius rolling ball method was used to reduce variability in brightness due to background. The continuity of the microtubule signal was improved visually by sequential Gaussian blur and unsharp mask steps. All of the image processing used standard features of ImageJ that were applied equally to the entire montage image, and none of the steps had a detectable effect on the measured microtubule network orientation outputs. To obtain estimates of the overall microtubule network within a region of interest that included the microtubule pattern of the entire branch, the ImageJ plugin OrientJ (23) was used. Mean microtubule orientations were measured for 121 trichomes using the following bins to define each class (0° and 180° oriented parallel to the long axis of the cell): longitudinal, 0°–14° and 166°–180°; transverse, 75°–105°; left-handed helical 15°–74°; right-handed helical 106°–165°.

Plant materials, growth conditions, trichome stage definition, and desiccation

The *Arabidopsis* (*Arabidopsis thaliana*) Columbia and Ler ecotypes were used to observe trichome behavior under turgor pressure removal. For all experiments, a range of branch lengths from young trichomes (branch lengths less than 50 μm) to old trichomes (branch lengths longer than 300 μm) was examined during desiccation with time-lapse imaging. Seeds were stratified at 4°C for 2 days and then grown in a growth chamber for 2 to 22 days under 12-h day length at 24°C and relative humidity of 50%–60%. The goal was to study different trichome branches with many different lengths.

Complete removal of the turgor pressure was needed to measure the amount of twist with respect to branch length. For slow desiccation, the whole plant was kept in soil at room temperature for about one month without watering (this duration may be different if this protocol were to be executed in a different facility due to the difference in humidity levels and months of the year). During this time, the plants were exposed to day and night light conditions in which the plant was naturally grown. Using this desiccation process, the cell persistently lost water, which led to the collapse and twist of trichomes. For fast desiccation, a vacuum was applied for 20 min that decreased the pressure from 1 to ∼0.05 mbar. All branches within each image were analyzed with respect to their twist with 570 branches measured overall (227 with slow desiccation; 343 with fast desiccation). To identify the direction of twist only, removal of a fraction of the cell water content was sufficient because the direction of twist was evident even after partial dehydration. A plastic Petri dish (2 and 3.5 in) was prepared, and the bottom of the plate was covered with strips of double-sided tape. Each leaf was trimmed from its attachment to the petiole. If the first and second leaves were the last or the last visible leaves, the whole plant was trimmed from its attachment to the root to avoid any possible damage to the leaves. The empty spaces between the leaves were filled with desiccant beads (silica gel desiccants 2.25 x 1.5 inches) to expedite the moisture removal. If the leaves were not visible by the naked eye and only observable under a 10× microscope, less than one day (∼10 h) was required to remove the turgor pressure and observe the direction of the twist. Typically, it took more than 10 days for the older and larger leaves or the trichomes farther away from the petiole to dry out and twist. Finally, after sufficient time (depending on the size of the leaf and the position of the trichome), the direction of twist was visible using a 20× lens of a laser scanning confocal microscope. Scanning electron microscopy (SEM) was useful for this study only for fully developed leaves and trichomes. At those stages of growth, enough space existed between trichomes for imaging. For small leaves, the SEM vacuum resulted in tangling of trichomes and bending of the

leaf such that high-quality images were challenging. The amount of twist for each range of branch length was measured by selecting a point on one of the edges of the collapsed trichome branch and moving along the path of the edge and measuring the amount of sweep angle. For a better understanding, see Fig. S2*A* and *B* that show the method used to measure the length and amount of twist, respectively.

Finite element model

An FE model of the trichome branch response to desiccation was created using the commercial finite element software Abaqus 2019. Several factors, including geometry, material properties, and boundary conditions, play a role in the deformation pattern after turgor pressure removal. The model parameters were adjusted to match the amount and direction of twist of the branches at different stages of growth (i.e., length). A more detailed description of the FE model, including the sensitivity study for mechanical properties and estimates of shear strain, is included in the Supporting Material. The trichome branch was modeled as a composite shell in which the branch diameter at the flank was constant with a radius of 8 μm (16). The cell wall was modeled as an orthotropic laminate composite with single dominant fiber orientation. The fiber direction was determined for a given branch length to match the amount of twist measured in the experiments. A layer of viscoelastic matrix, representative of the pectin in the wall, defined the time-dependent behavior of the cell wall using values based on pavement cell viscoelastic properties (24,25). The matrix modulus and modulus of the orthotropic layer perpendicular to the cellulose fibers were assumed as 100 MPa (26), and the modulus of the orthotropic layer parallel to the fibers was assumed as 70 GPa (27–30). Assuming a Poisson's ratio of 0.45 resulted in a shear modulus in all directions of 45 MPa. The wall matrix was assumed to constitute ∼36% of the cell wall with a density of 1000 kg/ m^3 (31), and the remaining volume was assumed to be occupied by cellulose (32), with a density of 1650 kg/ m^3 (29), which results in a density of the whole cell wall of 1416 kg/ m^3, consistent with measurements (33). The homogenized elastic properties were ∼45 GPa in the direction of fibers and ∼100 MPa perpendicular to the fibers, values close to the range from Gibson (34). The trichome branch was modeled as a shell reservoir under constant hydrostatic turgor pressure with a pressure on the outer wall to represent atmospheric pressure (0.1 MPa). The turgor pressure in the model was increased from 0 to 0.6 MPa, held constant for ∼20s, and then removed at the same rate as the increase. At this point, the branch was subjected to atmospheric pressure alone. A nonlinear analysis was implemented to model the large deformation after desiccation. Previous models of trichome branches provided little insight into the appropriate mechanical properties that were necessary to demonstrate the same twist after the removal of turgor pressure. Thus, the branch model was constructed based on the trichome branch shape, and the model properties were iterated to find the fiber orientation that reproduced the measured behavior. A comparison of values from experimental measurements and values used in the FE model is provided in Table S1, and the details of parameters used in the FE model are given in Table S2. An example FE model is accessible for download at https://github.com/Turner-TULiPS.

RESULTS AND DISCUSSION

Trichome branch twist reveals cell wall organization

Changes in the shape of individual trichome branches (*A. thaliana* WT Col-0) were studied and quantified by applying slow or fast desiccation treatments (Fig. 1; see supporting Video S1). The slow approach resulted in complete removal of turgor pressure as quickly as a few hours or as long as ∼30 days depending upon leaf age and the cell position relative to the petiole. The fast desiccation treatment (∼20 min; see Materials and Methods and Fig. S2) showed that the twist was not affected by possible reorientation of CMFs during the dehydration process. The geometry of the branch was symmetric about its long axis (i.e.,

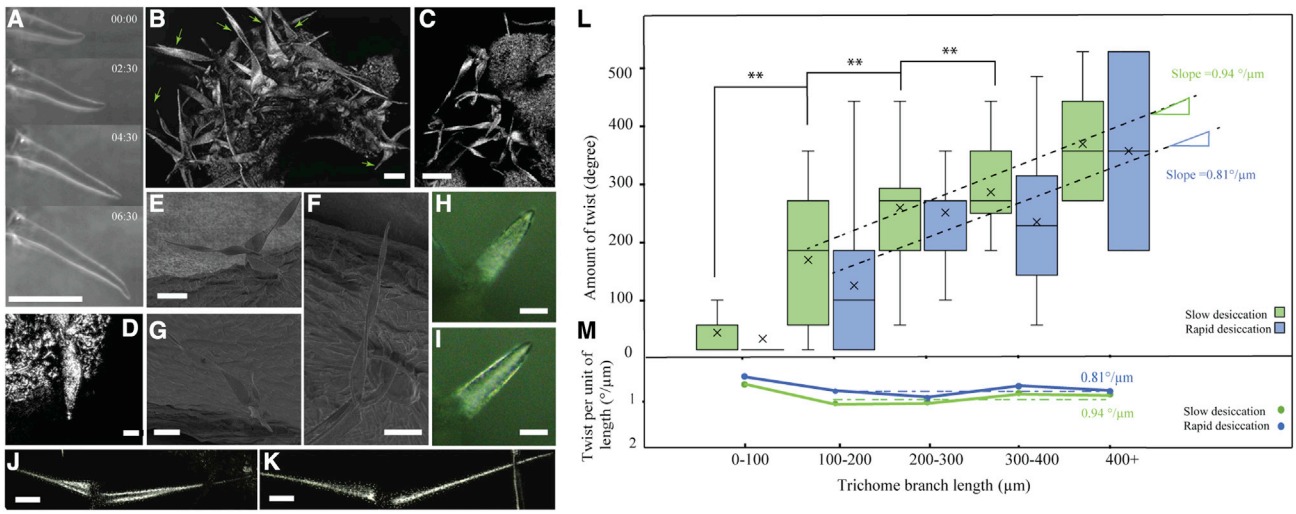

FIGURE 1 Twist of trichome branches during collapse after desiccation. (*A*) axisymmetric growth of leaf trichome branches (presented with permission from *Nature Plants* (16)) in 6 h and 30 min (*B*) and (*C*) are twisted trichome branches of *Arabidopsis* WT (Col) after desiccation. Arrows in (*B*) denote these branches. (*D*) Right-handed twist of a short trichome branch observed in less than 5% of the branches and only when they were short. (*E–G*) Left-handed twist of trichome branch imaged using SEM. (*H*) and (*J*) Trichome branch after dehydration. (*I*) and (*K*) The trichome branch in (*H*) after rehydration (∼2 h in water), which shows that the collapse of branches is elastic and recoverable; plastic deformation is not observed in the dehydration process. (*L*) Amount of twist and (*M*) twist per unit of length of desiccated branches for each range of length (in ° and °/μm respectively), from measurements of more than 570 trichome branches with slow and fast desiccation methods. **$p < 0.01$. Scale bars represent 40 μm in (*A*)–(*K*). To see this figure in color, go online.

axisymmetric) for all lengths (Fig. 1 *A*). However, the observed twist after desiccation was not possible unless the wall had an organization that was asymmetric. An image of a collection of trichome branches (Fig. 1 *B* and *C*) shows the consistency of the behavior after desiccation. The amount and direction of their twist were measured as a function of branch length. Interestingly, there was a clear length dependence to the twisting that occurred only for branches longer than ~100 μm. Branches shorter than this value (Fig. 1 *D*) showed minimal twist suggesting an axisymmetric organization of the cell wall. A right-handed twist was observed at this stage in only a small number of branches (less than 5%). On the other hand, 91.8% of branches with length >100 μm (Fig. 1 *E–G*) showed a clear twist, and the remaining 8.2% showed a collapse without twist. The twisted branches were left-handed for all but two branches (they had lengths of 108 and 113 μm). The branches in early stages (<100 μm length) recovered their original shape after rehydration (Fig. 1 *H–K*), which suggested that the response was elastic and reversible. This behavior may indicate an efficient mechanism for shape recovery during or after acute water stress. The twist per unit length (see supporting material) became a constant value of 0.81°/μm (fast desiccation) or 0.94°/μm (slow desiccation) (Fig. 1 *L*) for branches longer than the transition length (~100 μm), indicating that the wall organization was consistent with growth. The maximum amount of twist per unit of length (Fig. 1 *M*) increased from ~0.5°/μm to ~1°/μm when the mean branch length was about 150 μm and then dropped to ~0.81°/μm for branches longer than 400 μm.

Finite element model of a trichome branch

An FE model was used to estimate the mechanical properties that would lead to the observed twist behavior. Although direct measurements of plant pavement cells have been made using nanoindentation (24,25,35), atomic force microscopy (36–39), and other related devices (40), such approaches are challenging with trichome branches because of their location above the plane of the leaf. For this reason, the initial cell wall material properties for the model were based on direct measurements from pavement cells (16). The FE model was then used parametrically to identify the ranges of material properties and organization (i.e., elastic moduli, fiber orientation) that were plausible relative to the deformations observed. Although there was an inherent nonuniqueness to this analysis (i.e., multiple values of properties may result in the same behavior), overall behavior could be quantified because the direction of anisotropy was the primary factor that defined the twist. To find a plausible set of material properties, different combinations of properties were assumed, and the results were compared with the deformations observed in desiccated trichome branches. The loading conditions for the model were defined using the turgor pressure, which was increased to a maximum value and held constant for a consistent amount of time, which allowed the viscoelastic branch wall to relax fully. Then, the turgor pressure was removed so that the external atmospheric pressure was the only remaining applied force, which collapsed the branch. The relaxation process allowed residual stresses to develop in the cell wall. In arteries (17,18), the growth-induced residual stresses and material properties determine the opening angle of the orthotropic structure after a single cut is made. By analogy, residual stresses in the cell wall develop during growth as part of the expansion process and their status is revealed by the desiccation. The trichome branches undergo large deformations after desiccation such that a nonlinear solver for large deformation behavior was used in the FE model.

The cell wall includes many constituents such as cellulose microfibrils, pectin, hemicelluloses, and different proteins (5,41). Computational models of plant cells must account for these constituents in some way. Their length scale relative to the cell size dictates either high-resolution and massive computational models with limited scope or models based on material homogenization, such as that used here, that allow extensive parametric studies to be conducted. Thus, the trichome branch cell wall was modeled as a homogenized composite shell with mechanical properties derived from cellulose and pectin in which the orientation of cellulose fibers was allowed to vary with respect to position (Fig. 2 *A*; discussion of the sensitivity study is given in the Supporting Material). The properties of each element of the model were homogenized from the assumed composite organization to include both anisotropic and viscoelastic behavior. The direction of the anisotropy for the CMF orientation is denoted as $\hat{\mathbf{n}}$ such that 90° aligns with the branch longitudinal axis and 0° with the radial direction. The viscoelastic properties, representative of the pectin-rich matrix, defined the time-dependent behavior of the cell wall (25). Cell wall thickness plays an essential role in the overall trend concerning the twist along the length of the trichome (Fig. 2 *B*). Previous measurements of *Arabidopsis* trichoblasts (16) showed the presence of a thickness gradient from the tip toward the base, but those measurements focused on the early stages of growth and cell shape patterning. If a thickness gradient was used over the entire branch length, the FE models showed that the twist behavior was attenuated toward the base (Fig. 2 *B*), suggesting a uniform thickness in longer branches along the majority of the length away from the tip (see Supporting Material). The layered, composite organization used here could include any number of layers and organization (Fig. 2 *A*). We focused on a three-layer composite to represent the "average" wall behavior to simplify the quantification relative to the measurements. In this way, the trends with respect to length could be observed (Fig. 2 *C* and *D*). As expected, the amount and direction of branch twist depended

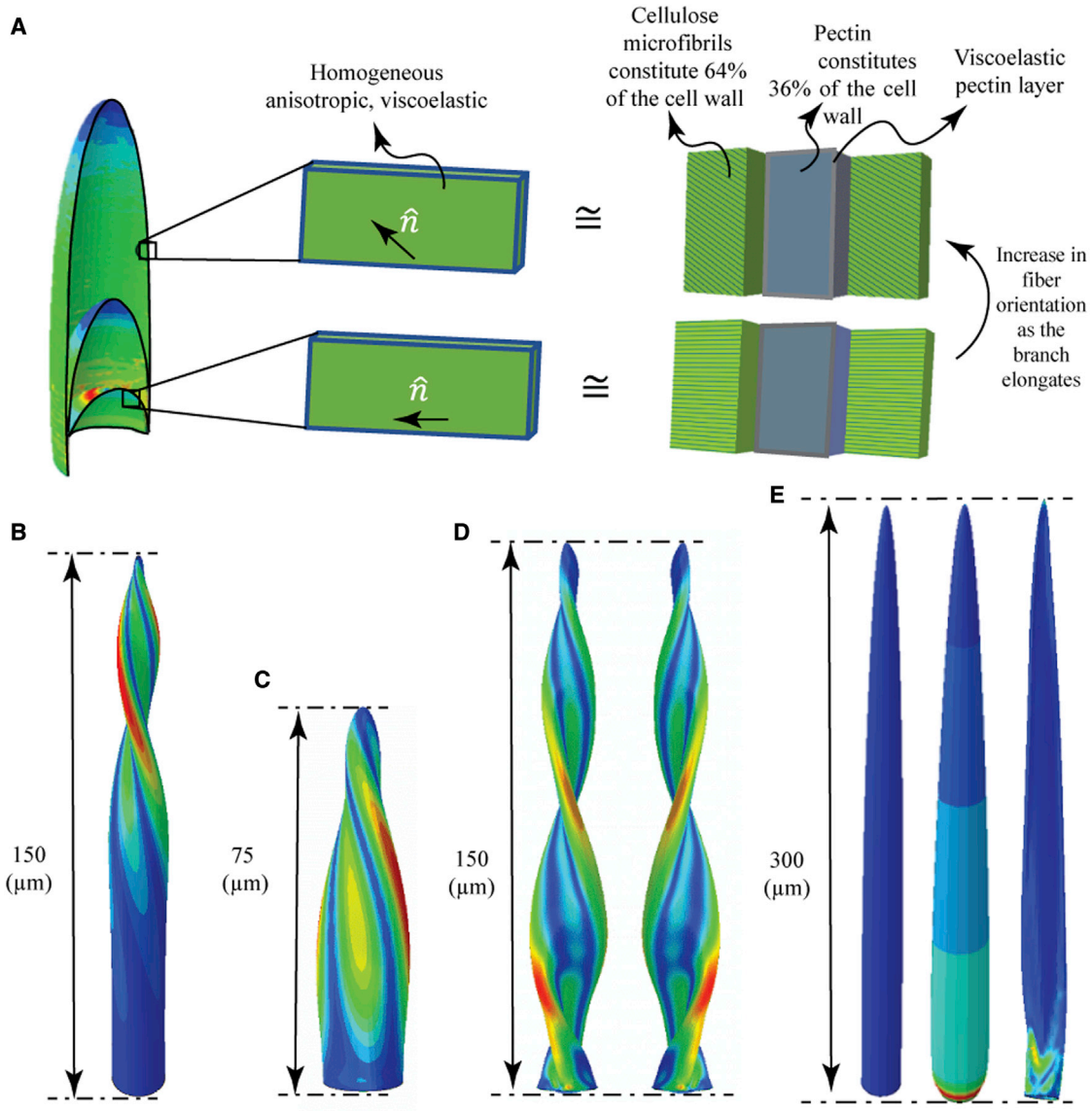

FIGURE 2 Finite element model of a trichome branch. (*A*) The organization of the cell wall is modeled as a composite shell of orthotropic and viscoelastic layers to represent the cellulose and pectin components, respectively, for different branch lengths. (*B*) Effect of the thickness profile on branch twist; if the cell wall thickness increases continuously from the tip to the base the twist is confined to the tip only; a constant thickness of 200 nm for positions more than 50 nm from the tip leads to the same twist observed in experiments. (*C*) and (*D*) Cell wall von Mises stress of the trichome branch model after removal of turgor pressure for branch length of 75 and 150 μm with dominant angle of −30° and −45° and +45°, respectively. Effect of right-handed fiber orientation on the direction of twist is shown in (*D*). (*E*) FE model of trichome branch with all longitudinal fibers without pressure (left), swelled under constant pressure without any longitudinal strain (middle), and star-shaped collapse after removing the pressure (right). To see this figure in color, go online.

upon fiber orientation, whether left-handed or right-handed (Fig. 2 *D*), with similar stress patterns. Based on the twist data, longer trichomes must have a higher percentage of fibers aligned more closely with the growth axis than shorter trichomes. However, if all fibers were oriented parallel with the branch longitudinal axis, the model predicted wall collapse without twist (Fig. 2 *E*), i.e., an axisymmetric collapse. Thus, the observed twist cannot be explained using fibers aligned only with the direction transverse to the longitudinal axis (circumferential) or aligned with it (axial).

Microtubule handedness is consistent with twist

The handedness of the twist of longer branches was clearly biased in the left-hand direction and highlighted the asymmetry in the cell wall that must be present. The angle of cortical microtubule orientation can be used as an additional validation of the model because microtubules and cellulose synthase (CESA) complexes are highly correlated in trichome branches (16). Live-cell microtubule imaging of entire branches was achieved by creating a montage of several high-resolution images that spanned the entire branch

length (Fig. 3 *A–D*) to reveal clear patterns of cellular scale cortical microtubule organization. As previously reported (42), shorter branches had more transversely aligned microtubules, whereas the orientation showed a directionality for longer branches. A bias toward left-handed asymmetry in trichome branch microtubule networks had been reported

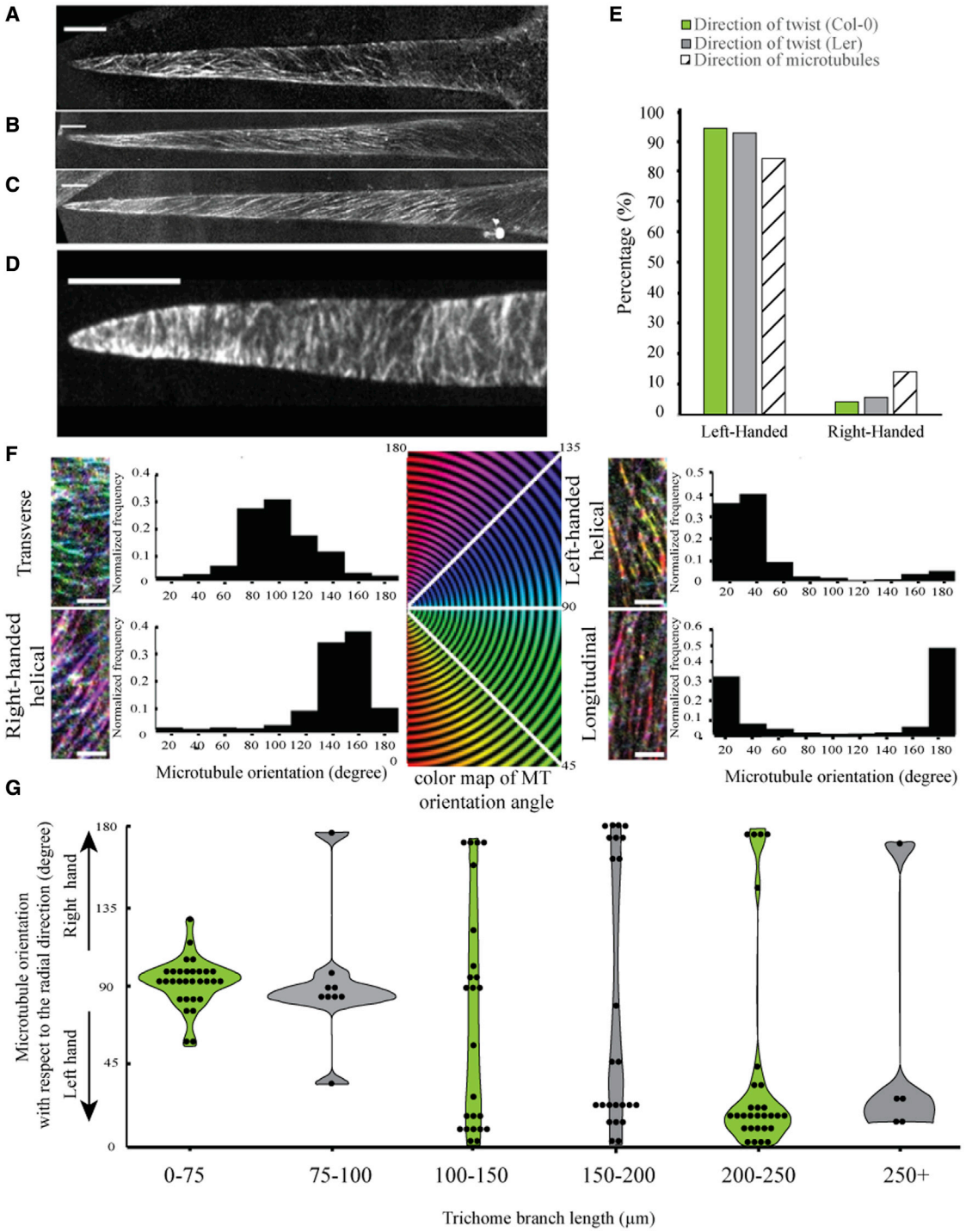

FIGURE 3 Microtubule alignment and handedness of helical arrays at different stages of growth. (*A–D*) Example projections of montage images of cortical microtubules in an entire branch, (*A*) dominant right-handed helices; (*B*) longitudinal dominance; (*C*) dominant left-handed helices; (*D*) net transverse alignment. (*E*) Strongly biased left-handed twist of desiccated branches (slow approach) in Col-0, Ler and the strong bias toward left-handed microtubule helices in trichome measurements. For fast desiccation (Col only), 100% of branches with twist showed left-handed bias. (*F*) Examples showing a global bias of microtubule alignment in the four alignment classes. (*G*) Dominant angle of the microtubule alignment relative to the primary growth axis. Scale bars represent 20 μm in (*A*)–(*D*) and 2 μm in (*F*). To see this figure in color, go online.

(43), but those measurements were limited with respect to trichome branch length and the fraction of the branch surface that was analyzed. We conducted high-resolution live-cell imaging of the cortical microtubule network of half of the branch cortex along its full length by tiling the individual images (Fig. 3 *A*). At whole branch scales the microtubule array often had a clear predominant orientation (Fig. 3 *A–D* and *F*); however, subdomains with mixed orientations were often observed. The microtubule organizations in 121 trichomes were categorized based on the mean microtubule orientation in the image field using the OrientJ plugin in ImageJ. Angles were defined with 0° and 180° oriented parallel to the long axis of the branch; longitudinal of 0°–14° and 166°–180°; transverse of 75°–105°; left-handed helical of 15°–74°; and right-handed helical of 106°–165°. Fig. 3 *G* reveals a distinct change in organization from transverse in cells <100 μm to a most frequently left-handed helical array in branches >100 μm. Of the 35 trichomes with a branch length greater than 100 μm and a uniform orientation, 87% had a left-handed helical organization (Fig. 3 *E*). Clearly, the microtubule patterning, as a pathway for CMF synthesis, exhibited a bias that was consistent with the branch twist behavior and was dominated toward the left-handed orientation. The consistency of trichome twist direction and handedness of microtubules showed a preferred asymmetry for branch wall organization similar to the crystal texture of other systems in nature, such as giant barnacle shells (44).

Branch stiffness and natural frequency

During branch growth, the new CMFs are synthesized in different directions. The fiber orientations that matched the twist behavior with respect to branch length are shown in Fig. 4 *A*. The orientation is transverse (0°) to the branch longitudinal axis when the branch is short. Then the orientation shifts with growth. The overall organization will affect the axial stiffness of the branch, defined as a weighted average of the material stiffness in the growth direction over the cross-sectional area of the wall (left schematic of Fig. 4; calculations provided in Supporting Material). Fig. 4 *B* shows the computed axial stiffness as a function of branch length for the Col trichome branches based on the models that matched the twist data. The stiffness initially decreases as a function of branch length due to the dominance of transverse CMFs and corresponding lack of twist in desiccated branches. The black trend line shows the prediction for axial stiffness if the CMFs remained transverse for all lengths. In longer branches, the axial stiffness increases because the CMFs are aligned more closely with the growth axis (see Fig. 4 *A*). The material displacement and stress at the base of the branch will be affected by the axial stiffness (i.e., higher stiffness will lead to lower displacement for the same turgor pressure). The model predicts that the longest branch would have an axial stiffness of ∼110 N/m (the symbol indicated with an *A* in Fig. 4 *B*). At this point, it is unclear if this value has biological meaning with respect to trichome growth.

The mechanism for the change in CMF orientation observed after the transition length of 100 μm was examined using the model. An axisymmetric organization of CMFs in the wall, whether transverse to the branch longitudinal axis or aligned with it, would result in wall stresses that also reflect this axisymmetry. In other words, the principal stresses would align with the axial and transverse directions during the early stages of growth. Such an axisymmetric wall stress or strain could not induce an asymmetric CMF synthesis, nor could it cause a passive realignment of existing CMFs. However, as the branch extends beyond a threshold value, the length itself could provide a mechanism to break the symmetry. The axial stiffness of the branch (Supporting Material) scales linearly with the axial modulus and inversely with length ($\sim L^{-1}$). The bending stiffness (right schematic of Fig. 4) also scales linearly with axial modulus, but inversely with the *cube* of the length ($\sim L^{-3}$). In other words, as the branch grows with constant properties defined by the transverse CMF alignment, it becomes more susceptible to bending motion that would shift the direction of maximum principal stress in the cell wall and break the symmetry. This shift, in turn, could influence microtubules and the angle of cellulose fiber synthesis. Results from the Col FE model (solid lines in Fig. 4 *B*), based on an assumption of only transverse CMFs, show the trend for both axial stiffness and bending stiffness with respect to branch length. The model predicts that a branch of length ∼100 μm would have a bending stiffness of ∼0.08 N/m (symbol indicated with *B* in Fig. 4 *B*). Remarkably, models created to match the measured twist data predict a bending stiffness for longer branches that plateaus to a constant value. Ambient environmental variations, such as thermal noise, could strongly influence such a compliant structure. A similar type of thermal noise is often exploited to calibrate atomic force microscope cantilevers (45) that can be much stiffer (∼40 N/m), but more resonant. The estimated bending displacements of tens to hundreds of nanometers would be enhanced at the branch tip as tapering occurs due to the reduced cross-section. After the synthesis of oriented CMFs is initiated, the subsequent growth would never return to the condition of axisymmetric synthesis, and the principal stresses would remain unaligned with the branch longitudinal axis. The reason for the left-hand bias cannot be ascertained at this point. At subsequent stages of growth, the shear stress could also cause some degree of passive reorientation of CMFs (14). A combination of a bending motion, the progressively decreasing cell diameter during the tapering process that could affect microtubule stability (46), or the disappearance of tip-localized cytoskeletal regulators (16,47) may explain the length associated with the symmetry-breaking event that dramatically alters microtubule and CMF synthesis patterns. The degree of twist and direction of twist are controlled by cytoskeletal (48) and

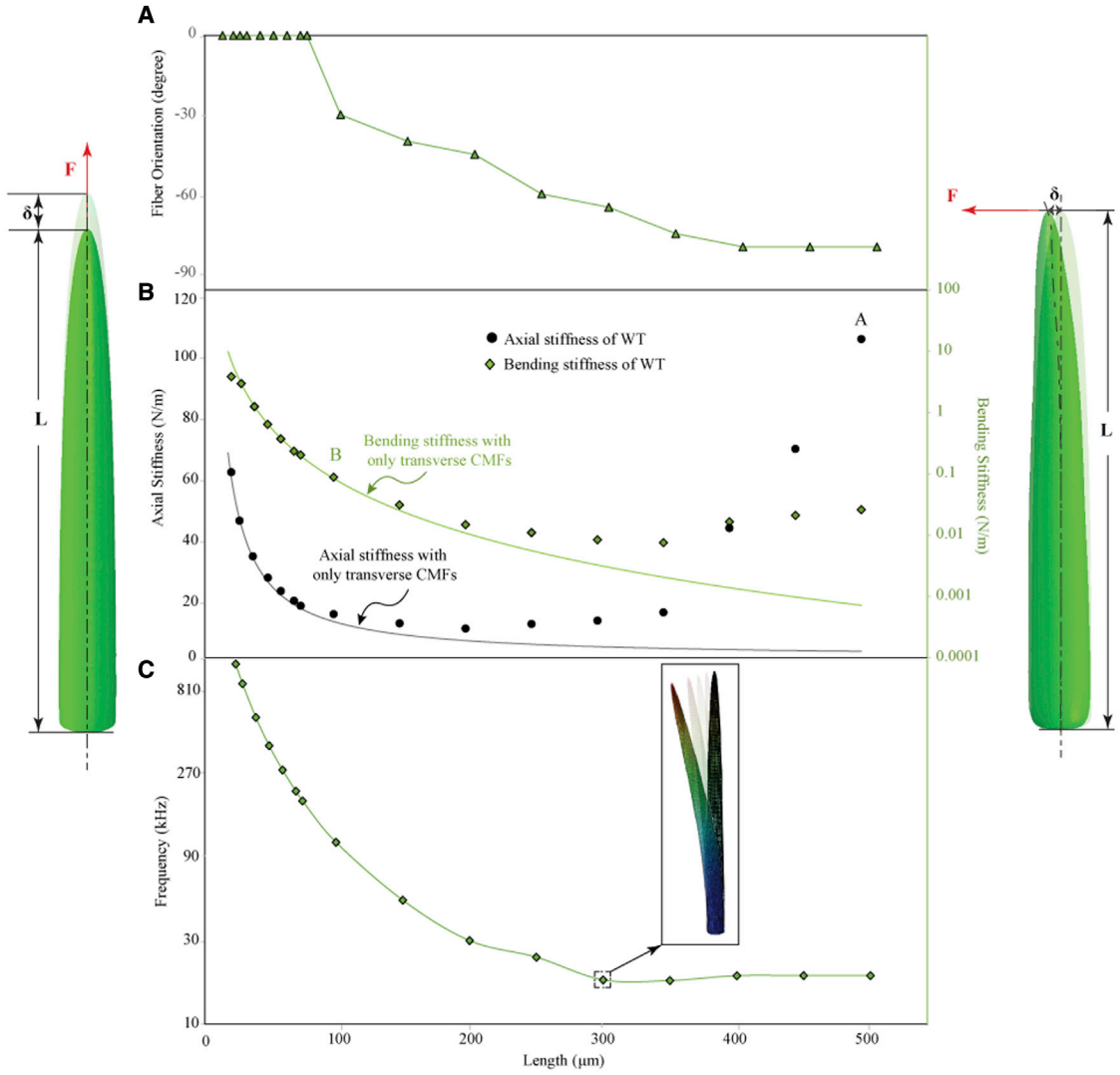

FIGURE 4 Influence of cellulose microfibril (CMF) orientation on bending stiffness, axial stiffness, and natural frequency of the first vibration mode. (*A*) Fiber orientation angle necessary to match the observed branch twist behavior. (*B*) Predicted axial and bending stiffness of trichome branches with different lengths based on model values needed to match twist data. Solid lines show predicted trends of axial and bending stiffnesses if CMF orientation remained transverse for the entire length. Axial stiffness (see Supporting Material) converges to about 100 N/m at point *A*, which suggests that growth stops when the value of axial stiffness is reached. Bending stiffness for WT trichome branches shows an initial reduction but then a stabilization as a function of length. After a length of about 100 μm, when the bending stiffness reaches the minimum possible value, the CMF deposition is no longer transverse to the branch longitudinal axis, which stabilizes the influence of bending even for longer branches. (*C*) First natural frequency of bending vibration for the branch based on the model values needed to match the twist data (note: the vertical axis is logarithmic). The frequency asymptotes to ~20 kHz after a length of ~300 μm. To see this figure in color, go online.

cell wall biosynthesis (49) systems that have poorly understood effects on cell wall patterning and morphogenesis. The approach described here provides a reliable strategy to integrate cell growth and desiccation phenotypes with biomechanics and their genetic control.

The results presented also suggest a limit to the hypothesis regarding passive reorientation. The multinet growth hypothesis suggests that cell wall elongation or expansion modifies the organization of CMFs that are exposed to shear stress in the cell, potentially resulting in passive reorientation toward the growth direction (14,39). For a longitudinal strain of 14%, the average orientation of wall polymer chains of onion was observed to rotate along the stretch direction by ~5.3 ° (50). However, this tilt and realignment of CMFs have not been observed in all cell types. For example, live-cell imaging of *Arabidopsis* was used to analyze cellulose reorientation during root cell growth in WT seedlings (51). No evidence of reorientation was detected in a mutant, *procuste1-1* (*prc1-1*) with a partial defect in cellulose synthesis. Complete reorientation of all microfibrils to the symmetry direction would not support the twist measured here. After the left-handed deposition initiates, additional elongation of the branch would be accompanied by some reorientation of CMFs, which would enhance the axial stiffness of

the branch. This behavior is thought to decrease the net growth rate of the cell, and eventually cease the growth process (51). By observing the growth of the WT *Arabidopsis* trichome branch, it was clear that the growth rate was almost constant during the first 50 μm. This rate increased for some later periods of growth but never fell below the initial rate (16). The growth rate should be correlated with the CMF orientations, a subject for future investigations. Analysis of helical growth from *Arabidopsis* mutants such as the *tor2* or *tor2 zwichel* double mutant indicated that microtubules play a significant role in the helical phenotype of leaf trichomes (52). *Arabidopsis* mutants growing with a right-handed twist have been reported to have cortical microtubules that are oriented around the cell in left-handed helices and vice versa (53). The relationship between microtubules and the direction of cell growth is usually explained by assuming that microtubules control the deposition of load-bearing cellulose microfibrils of the cell wall, so the cells elongate or expand in a direction perpendicular to the deposited cellulose (16). Furutani et al. (52) used this model to explain helical growth in spiral mutants for which expansion perpendicular to cellulose fibers that are synthesized in a left-handed direction would result in right-handed growth and vice versa. Others explain the behavior as a helix that unwraps in the direction opposite to the direction of stretch so that a wall generated with a left-handed helical pitch would unwind with a right-handed twist as the cell elongates (54). The results here suggest that the helical growth observed in mutant trichome branches (55) cannot be the result of microtubule handedness alone because the handedness of synthesis in the WT gives rise to a straight branch.

Finally, the first natural frequency of trichome branch bending was calculated based on the model values that matched the twist behavior (Fig. 4 *C*). The results show a convergence to a constant value of ∼20 kHz as the branch reaches the length of ∼300 μm. The vibration frequencies of leaf trichomes have been shown to correlate with protection of the leaves against insects such as caterpillars (19,20). Previous models of trichome vibrations (19,20) predicted frequencies above the range of many insects (56–58), but those models were based on a thicker cell wall (1.5–6 μm) (59), isotropic properties, and lower cell wall stiffness (0.6–4.7 GPa) (34,60). They also assumed that the properties were constant during growth. Our results based on the twist observations as a function of growth show that the frequencies would plateau when the branch reaches full maturity and lie within the frequency band of feeding, courtship, and communication of several insects including caterpillars (19,20), crickets (56), katydid (57), and cicadas (58).

Limitations

This study had some limitations that are worth noting. Our study did not include direct observations of the CMFs themselves. Ideally, cross-sectional maps are needed to quantify the organization of the CMFs with respect to position within the branch cell wall (radially and axially). The known correlations between microtubules orientation and CMFs does provide some confidence in the results, although the microtubules represent only the CMFs synthesized at the inner surface of the cell wall. A simply three-layer composite model was able to reproduce the twist observations, but more sophisticated models may be needed. In addition, the computational model required several parameter assumptions that are difficult to verify. In particular, the wall thickness variation was assumed fixed, and the wall properties were assumed to be uniform. The sensitivity study provides details regarding the impact of the assumptions, but additional experiments are needed to quantify cell wall properties directly. Such experiments are challenging as well if the full anisotropic, viscoelastic behavior of trichome branches is to be quantified fully. Clearly, more research is needed on several fronts.

CONCLUSION

In this article, we have presented a predictive computational model that replicates the mechanical twist of desiccated trichome branches to provide insight into the organization of constituents within the branch cell wall that change during growth. The presence of an asymmetric organization is hidden by the axisymmetric geometry of the pressurized branch. The FE model was used to quantify the observations of the branch twist that revealed the changes that occurred during growth, and the microtubule imaging validated the wall organization necessary for twist. The observed behavior cannot be the result of CMF reorientation or changes due to cell wall decomposition during the desiccation process because the twist was present even for fast desiccation. These observations do not support strong passive realignment of CMFs, although it may be present to some extent after the transition point of ∼100 μm at which time CMF synthesis asymmetry initiates. Shorter branches have only transversely oriented CMFs, and such an organization would have principal stresses aligned with the axial and transverse directions. The length of the transition of CMF orientation corresponds with a predicted branch bending stiffness, based on models created to match the measured twist, that would allow ambient noise of the plant and environment to induce bending displacements of the branch.

Our results firmly establish that removal of turgor pressure can reveal salient information about cell wall composition, which can improve the interpretation of genetic and environmental effects on plant growth. Desiccation of cells has been used by others recently (61) to test hypotheses about changes in cell wall organization during growth. They showed that dehydration of cotyledons led to wrinkling of the periclinal cell walls, whereas anticlinal walls were affected much less. If more accurate information about

cell wall mechanical properties can be determined by means of desiccation, imaging, and computational models during growth, then more accurate predictions can be made regarding overall static and dynamic behavior. Further research and multiscale models are needed to understand the role of mechanical stress on individual cell wall constituents to predict growth mechanics more accurately.

SUPPORTING MATERIAL

Supporting material can be found online at https://doi.org/10.1016/j.bpj.2022.02.013.

AUTHOR CONTRIBUTIONS

All authors participated in the experimental design, data collection, data analysis, and manuscript preparation. J.A.T. conceived the project. J.A.T. and S.K. developed the finite element models. S.K. conducted the branch imaging and data processing. T.D. performed the microtubule measurements under the guidance of D.B.S.

ACKNOWLEDGMENTS

We thank to the Purdue Life Science Microscopy Facility for their expert assistance. We thank the Nano-Engineering Research Core Facility (NERCF) for their high-performance microscopy and we acknowledge the Holland Computing Center (HCC). Both NERCF and HCC are supported in part by the Nebraska Research Initiative. This research was supported by NSF Grant No. IOS-1715444 to D.B.S. and J.A.T. The authors declare no conflict of interest.

SUPPORTING CITATIONS

References (62–64) appear in the Supporting material.

REFERENCES

1. Somerville, C. 2006. Cellulose synthesis in higher plants. *Annu. Rev. Cell Dev. Biol.* 22:53–78.
2. Fujita, M., R. Himmelspach, …, G. O. Wasteneys. 2013. The anisotropy1 D604N mutation in the Arabidopsis cellulose Synthase1 catalytic domain reduces cell wall crystallinity and the velocity of cellulose. *Plant Physiol.* 162:74–85.
3. Paredez, A. R., C. R. Somerville, and D. Ehrhardt. 2006. Visualization of cellulose synthase with microtubules. *Science.* 312:1491–1495.
4. Geitmann, A., and J. K. E. Ortega. 2009. Mechanics and modeling of plant cell growth. *Trends Plant Sci.* 14:467–478.
5. Cosgrove, D. J. 1999. Enzymes and other agents that enhance cell wall extensibility. *Annu. Rev. Plant Physiol. Plant Mol. Biol.* 50:391–417.
6. Baskin, T. I. 2005. Anisotropic expansion of the plant cell wall. *Annu. Rev. Cell Dev. Biol.* 21:203–222.
7. McFarlane, H. E., A. Döring, and S. Persson. 2014. The cell biology of cellulose synthesis. *Annu. Rev. Plant Biol.* 65:69–94.
8. Adoutte, A., and H. Le Guyader. 1993. The cytoskeletal basis of plant growth and form. *Plant Sci.* 88:125.
9. Verger, S., Y. Long, …, O. Hamant. 2018. A tension-adhesion feedback loop in plant epidermis. *Elife.* 7:e34460.
10. Robinson, S., and C. Kuhlemeier. 2018. Global compression reorients cortical microtubules in Arabidopsis hypocotyl epidermis and promotes growth. *Curr. Biol.* 28:1794–1802.
11. Belteton, S. A., W. Li, …, D. B. Szymanski. 2021. Real-time conversion of tissue-scale mechanical forces into an interdigitated growth pattern. *Nat. Plants.* 7:826–841.
12. Hamant, O., M. G. Heisler, …, J. Traas. 2008. Developmental patterning by mechanical signals in Arabidopsis. *Science.* 322:1650–1655.
13. Fischer, K., and P. Schopfer. 1997. Interaction of auxin, light, and mechanical stress in orienting microtubules in relation to tropic curvature in the epidermis of maize coleoptiles. *Protoplasma.* 196:108–116.
14. Green, P. B. 1960. Multinet growth in the cell wall of Nitella. *J. Biophys. Biochem. Cytol.* 7:289–296.
15. Preston, R. D. 1982. The case for multinet growth in growing walls of plant cells. *Planta.* 155:356–363.
16. Yanagisawa, M., A. S. Desyatova, …, D. B. Szymanski. 2015. Patterning mechanisms of cytoskeletal and cell wall systems during leaf trichome morphogenesis. *Nat. Plants.* 1:15014.
17. Alford, P. W., J. D. Humphrey, and L. A. Taber. 2008. Growth and remodeling in a thick-walled artery model: effects of spatial variations in wall constituents. *Biomech. Model. Mechanobiol.* 7:245–262.
18. Holzapfel, G. A., T. C. Gasser, and R. W. Ogden. 2000. A new constitutive framework for arterial wall mechanics and a comparative study of material models. *J. Elast. Phys. Sci. Solids.* 61:1–48.
19. Liu, S., J. Jiao, …, G. M. Genin. 2017. Arabidopsis leaf trichomes as acoustic antennae. *Biophys. J.* 113:2068–2076.
20. Yin, J., H. Liu, …, S. Liu. 2021. Ensembles of the leaf trichomes of Arabidopsis thaliana selectively vibrate in the frequency range of its primary insect herbivore. *Extrem. Mech. Lett.* 48:101377.
21. Szymanski, D., and C. J. Staiger. 2018. The actin cytoskeleton: functional arrays for cytoplasmic organization and cell shape control. *Plant Physiol.* 176:106–118.
22. Yu, Y., S. Wu, …, Z. Kong. 2019. Live-cell imaging of the cytoskeleton in elongating cotton fibres. *Nat. Plants.* 5:498–504.
23. Püspöki, Z., M. Storath, …, M. Unser. 2016. Transforms and operators for directional bioimage analysis: a survey. *Adv. Anat. Embryol. Cell Biol.* 219:69–93.
24. Forouzesh, E., A. Goel, …, J. A. Turner. 2013. *In vivo* extraction of Arabidopsis cell turgor pressure using nanoindentation in conjunction with finite element modeling. *Plant J.* 73:509–520.
25. Hayot, C. M., E. Forouzesh, …, J. A. Turner. 2012. Viscoelastic properties of cell walls of single living plant cells determined by dynamic nanoindentation. *J. Exp. Bot.* 63:2525–2540.
26. Zsivanovits, G., A. J. MacDougall, …, S. G. Ring. 2004. Material properties of concentrated pectin networks. *Carbohydr. Res.* 339:1317–1322.
27. Cintrón, M. S., G. P. Johnson, and A. D. French. 2011. Young's modulus calculations for cellulose Iβ by MM3 and quantum mechanics. *Cellulose.* 18:505–516.
28. Diddens, I., B. Murphy, …, M. Müller. 2008. Anisotropic elastic properties of cellulose measured using inelastic X-ray scattering. *Macromolecules.* 41:9755–9759.
29. Mariano, M., N. El Kissi, and A. Dufresne. 2014. Cellulose nanocrystals and related nanocomposites: review of some properties and challenges. *J. Polym. Sci. Part B Polym. Phys.* 52:791–806.
30. Eichhorn, Y. R. J. 2001. The young's modulus of a microcrystalline cellulose. *Cellulose.* 8:197–207.
31. Guimarães, G. C., M. C. Coelho Júnior, and E. E. Garcia Rojas. 2009. Density and kinematic viscosity of pectin aqueous solution. *J. Chem. Eng. Data.* 54:662–667.
32. Taiz, L., and E. Zeiger. 2002. Plant Physiology, 3rd ed. Sinauer Associates, Sunderland, MA, pp. 313–338.
33. Wayne, R., and M. P. Staves. 1991. The density of the cell sap and endoplasm of nitellopsis and chara. *Plant Cell Physiol.* 32:1137–1144.
34. Gibson, L. J. 2012. The hierarchical structure and mechanics of plant materials. *J. R. Soc. Interf.* 9:2749–2766.

35. Li, W., S. Keynia, S. A. Belteton, F. Afshar-Hatam, D. B. Szymanski, J. A. Turner…, 2021. Protocol for mapping the variability in cell wall mechanical bending behavior in living leaf pavement cells. *Plant Physiol.* kiab588. https://doi.org/10.1093/plphys/kiab588.

36. Milani, P., V. Mirabet, …, A. Boudaoud. 2014. Matching patterns of gene expression to mechanical stiffness at cell resolution through quantitative tandem epifluorescence and nanoindentation. *Plant Physiol.* 165:1399–1408.

37. Xi, X., S. H. Kim, and B. Tittmann. 2015. Atomic force microscopy based nanoindentation study of onion abaxial epidermis walls in aqueous environment. *J. Appl. Phys.* 117:24703.

38. Marga, F., M. Grandbois, …, T. I. Baskin. 2005. Cell wall extension results in the coordinate separation of parallel microfibrils: evidence from scanning electron microscopy and atomic force microscopy. *Plant J.* 43:181–190.

39. Zhang, T., D. Vavylonis, …, D. J. Cosgrove. 2017. Nanoscale movements of cellulose microfibrils in primary cell walls. *Nat. Plants.* 3:17056.

40. Sugimoto, K., R. E. Williamson, and G. O. Wasteneys. 2002. New techniques enable comparative analysis of microtubule orientation, wall texture, and growth rate in intact roots of Arabidopsis. *Plant Physiol.* 124:1493–1506.

41. Burton, R. A., M. J. Gidley, and G. B. Fincher. 2010. Heterogeneity in the chemistry, structure and function of plant cell walls. *Nat. Chem. Biol.* 6:724–732.

42. Folkers, U., V. Kirik, …, M. Hülskamp. 2002. The cell morphogenesis gene ANGUSTIFOLIA encodes a CtBP/BARS-like protein and is involved in the control of the microtubule cytoskeleton. *EMBO J.* 21:1280–1288.

43. Sambade, A., K. Findlay, …, H. Buschmann. 2014. Actin-dependent and -independent functions of cortical microtubules in the differentiation of Arabidopsis leaf trichomes. *Plant Cell.* 26:1629–1644.

44. Rodríguez-Navarro, A. B., C. CabraldeMelo, …, J. L. Arias. 2006. Microstructure and crystallographic-texture of giant barnacle (Austromegabalanus psittacus) shell. *J. Struct. Biol.* 156:355–362.

45. Sader, J. E., J. W. M. Chon, and P. Mulvaney. 1999. Calibration of rectangular atomic force microscope cantilevers. *Rev. Sci. Instrum.* 70:3967–3969.

46. Ambrose, C., J. F. Allard, …, G. O. Wasteneys. 2011. A CLASP-modulated cell edge barrier mechanism drives cell-wide cortical microtubule organization in Arabidopsis. *Nat. Commun.* 2:1–12.

47. Yanagisawa, M., J. M. Alonso, and D. B. Szymanski. 2018. Microtubule-dependent confinement of a cell signaling and actin polymerization control module regulates polarized cell growth. *Curr. Biol.* 28:2459–2466.e4.

48. Ishida, T., Y. Kaneko, …, T. Hashimoto. 2007. Helical microtubule arrays in a collection of twisting tubulin mutants of Arabidopsis thaliana. *Proc. Natl. Acad. Sci. U S A.* 104:8544–8549.

49. Saffer, A. M., N. C. Carpita, and V. F. Irish. 2017. Rhamnose-containing cell wall polymers suppress helical plant growth independently of microtubule orientation. *Curr. Biol.* 27:2248–2259.e4.

50. Kafle, K., Y. Bum Park, …, S. H. Kim. 2017. Effects of mechanical stretching on average orientation of cellulose and pectin in onion epidermis cell wall: a polarized FT-IR study. *Cellulose.* 24:3145–3154.

51. Anderson, C. T., A. Carroll, …, C. Somerville. 2010. Real-time imaging of cellulose reorientation during cell wall expansion in Arabidopsis roots. *Plant Physiol.* 152:787–796.

52. Furutani, I., Y. Watanabe, …, T. Hashimoto. 2000. The SPIRAL genes are required for directional control of cell elongation in Aarabidopsis thaliana. *Development.* 127:4443–4453.

53. Yuen, C. Y. L., R. S. Pearlman, …, P. H. Masson. 2003. WVD2 and WDL1 modulate helical organ growth and anisotropic cell expansion in Arabidopsis. *Plant Physiol.* 131:493–506.

54. Lloyd, C., and J. Chan. 2002. Helical microtubule arrays and spiral growth. *Plant Cell.* 14:2319–2324.

55. Buschmann, H., M. Hauptmann, …, A. R. Schäffner. 2009. Helical growth of the Arabidopsis mutant tortifolia2 does not depend on cell division patterns but involves handed twisting of isolated cells. *Plant Cell.* 21:2090–2106.

56. Libersat, F., J. A. Murray, and R. R. Hoy. 1994. Frequency as a releaser in the courtship song of two crickets, Gryllus bimaculatus (de Geer) and Teleogryllus oceanicus: a neuroethological analysis. *J. Comp. Physiol. A.* 174:485–494.

57. Pollack, G. S., and K. Imaizumi. 1999. Neural analysis of sound frequency in insects. *BioEssays.* 21:295–303.

58. Bennet-Clark, H., and D. Young. 1994. The scaling of song frequency in cicadas. *J. Exp. Biol.* 191:291–294.

59. Zhou, L. H., S. B. Liu, …, B. G. Pickard. 2017. The Arabidopsis trichome is an active mechanosensory switch. *Plant Cell Environ.* 40:611–621.

60. Probine, M. C., and R. D. Preston. 1962. Cell growth and the structure and mechanical properties of the wall in internodal cells of Nitella opaca: II. MECHANICAL PROPERTIES OF THE WALLS. *J. Exp. Bot.* 13:111–127.

61. Haas, K. T., R. Wightman, …, A. Peaucelle. 2020. Pectin homogalacturonan nanofilament expansion drives morphogenesis in plant epidermal cells. *Science.* 367:1003–1007.

62. Chafe, S. C., and A. B. Wardrop. 2004. Fine structural observations on the epidermis. *Planta.* 109:39–48.

63. Dyson, R. J., and O. E. Jensen. 2010. A fibre-reinforced fluid model of anisotropic plant cell growth. *J. Fluid Mech.* 655:472–503.

64. Kubátová, Z., P. Pejchar, …, I. Kulich. 2019. Arabidopsis trichome Contains two Plasma Membrane Domains with different Lipid compositions which Attract distinct EXO70 Subunits. *Int. J. Mol. Sci.* 20:3803.